



Coupled flow and transport modelling of a large-scale *in situ* migration experiment with ^{14}C -labelled natural organic matter colloids in Boom Clay

Joan Govaerts^{1*}, Norbert Maes¹, Delphine Durce¹, Marc Aertsens¹ and Stéphane Brassinnes²

¹SCKCEN, Belgian Nuclear Research Centre, Institute for Environment, Health and Safety, Boeretang 200, B-2400 Mol, Belgium

²ONDRAF/NIRAS, Kunstlaan 14, B-1210 Brussels, Belgium

 JG, 0000-0003-4922-1704

*Correspondence: joan.govaerts@sckcen.be

Abstract: Twenty-five years ago, a unique long-term and large-scale *in situ* experiment with ^{14}C -labelled natural organic matter (NOM) was set up at the HADES underground research facility in Mol (Belgium) to study its migration behaviour. Natural organic matter plays an important role in the mobility of various safety-relevant radionuclides, which is critical in the context of Safety & Performance Assessment (SA/PA) calculations for a possible nuclear waste repository. The objective of this work is to enlarge the confidence in current NOM transport models by validating them with the *in situ* experiment, which is still continued to this day. Stepwise adding more complexity to the model resulted in a 10-parameter model with which excellent fits to the data are obtained. The model considers two different fractions that are transported by advection and diffusion and can be subject to both irreversible and reversible immobilization processes. The associated fitted parameter values compare well with values determined on small-scale migration experiments. This builds confidence in the NOM transport model, which in turn contributes to the confidence in the outcome of the radionuclide migration calculations performed in the context of SA/PA. These results again highlight the incredible value of such long-running experiments at underground research facilities like HADES.

Supplementary material: Supplementary figures and data are available at <https://doi.org/10.6084/m9.fig-share.c.6315969>

Any country deploying nuclear power plants for electricity production has to find a final solution for its high- and intermediate-level radioactive waste. The preferred option adopted by many countries for the long-term management of high- and intermediate-level radioactive waste and/or spent fuel is its disposal in a geological repository, in which a multibarrier system, combining natural host rock and engineered barriers, is foreseen. In Belgium, no formal decision on a host formation has been taken yet, but for R&D purposes, the Belgian radioactive waste management organization ONDRAF/NIRAS considers Boom Clay as one of the potential natural barriers for a geological disposal facility in poorly indurated plastic clays (ONDRAF/NIRAS 2013).

For this purpose, Boom Clay shows excellent properties: pronounced self-sealing capacity (Van Geet *et al.* 2008), a geochemical environment favouring low solubility combined with a substantial sorption capacity for various radionuclides (RNs) (Van Laer *et al.* 2016; Bruggeman and Maes 2017; Maes *et al.* 2021) and limited water flow (Yu *et al.*

2013). The low hydraulic conductivity and low hydraulic gradient (Yu *et al.* 2013) over the formation make molecular diffusion the dominant solute transport mechanism (Mazurek *et al.* 2011). As most radionuclides are prone to sorb on the clay minerals and likely to (co)precipitate in the clay porewater, radionuclide migration through the clay barrier is extremely slow.

However, Boom Clay is rich in natural organic matter (NOM) with total organic carbon values typically between 1 and 5 wt% while the porewater contains on average 115 mg C l⁻¹ of dissolved organic carbon (Maes *et al.* 2004; Bruggeman and De Craen 2012). Dissolved organic matter (DOM) is assumed to correspond to the fraction of organic carbon that is smaller than 0.45 µm (Zsolnay 2003). Natural DOM present in Boom Clay porewater displays a broad molecular weight distribution ranging from species of a few hundred Da to aggregates larger than 100 kDa. Owing to size exclusion, only a fraction of DOM is potentially mobile throughout the Boom Clay, which exhibits pore throat diameters down to c. 20 nm (Hemes *et al.* 2015), with most of

From: Li, X. L., Van Geet, M., Bruggeman, C. and De Craen, M. (eds) 2023. *Geological Disposal of Radioactive Waste in Deep Clay Formations: 40 Years of RD&D in the Belgian URL HADES*.

Geological Society, London, Special Publications, **536**, 145–158.

First published online February 20, 2023, <https://doi.org/10.1144/SP536-2022-22>

© 2023 The Author(s). This is an Open Access article distributed under the terms of the Creative Commons Attribution License (<http://creativecommons.org/licenses/by/4.0/>). Published by The Geological Society of London.

Publishing disclaimer: www.geolsoc.org.uk/pub_ethics

the mobile part being smaller than 20 kDa (Durge *et al.* 2015).

Many radionuclides (lanthanides, actinides, transition metals, etc.) show a high affinity towards DOM and form complexes/colloids (Dierckx *et al.* 1994; Moulin *et al.* 1995; Maes *et al.* 2003; Liu *et al.* 2008; Bruggeman *et al.* 2010). Consequently, the concentrations of these radionuclides in the clay porewater can be higher than their thermodynamic solubility. Moreover, they can also get attached to the mobile fraction of DOM and be transported with it. This phenomenon is called colloid-facilitated transport and can strongly enhance the long-term migration of otherwise hardly mobile radionuclides (Salah *et al.* 2015; Bruggeman *et al.* 2017a, b).

It is essential to quantify the migration behaviour of DOM to fully understand its contribution to the mobility of various safety-relevant radionuclides, in the context of safety and performance assessments (SA/PA). To this end, various lab-scale experiments were performed on Boom Clay cores to study the transport of DOM and derive transport models (Put *et al.* 1998; Durge *et al.* 2018). Long-term experiments that allow the study of DOM-linked migration of RNs, which clearly show this enhanced transport, were also performed and are described in the literature (Maes *et al.* 2011; Van Laer 2018).

A sound description of the migration of radionuclides that interact with DOM is of key importance for SA/PA calculations related to poorly indurated clays with high organic content (like the Boom Clay). Safety assessment calculations, as a part of the Safety Case for a geological waste repository, aim at quantitatively demonstrating the long-term radiological safety of the disposal system. They consist of a chain of model calculations assessing the release of radionuclides, their migration through the host formation, their dilution in surrounding aquifer layers, transfers between biosphere components and eventually health effects for a reference person. Performance assessment calculations aim at demonstrating the functioning of the integrated repository system and testing the robustness of the main engineered and natural barriers under different assumptions. Since the demonstration of safety relies heavily on porous media flow and transport models that deal with extreme timescales, it is of utmost importance to assure the validity of those models so that all stakeholders have confidence in the safety assessment outcome. In a recent update of the glossary, IAEA (2019) specifies that

modelling the behaviour of an engineered system in a (geological) disposal facility involves temporal and spatial scales for which no comparisons with system level tests are possible: models cannot be validated for that which cannot be observed. ‘Model validation’ in these circumstances implies showing that there is a

basis for confidence in the model(s) by ... comparisons with appropriate field and laboratory tests, and comparisons with observations of tests ... at the process level.

So, even if the model in its entirety cannot be validated, a partial validation is still possible. The most important processes of the model can be singled out, and compared with experimental data, *in situ* measurements and/or natural analogues. This is illustrated in the literature (Weetjens *et al.* 2014; Govaerts and Weetjens 2017), where the advective–diffusive transport of tracer radionuclides in a low-permeable porous medium (Boom Clay) is numerically modelled and compared with a long-term *in situ* migration experiment at HADES underground research laboratory (URL).

The objective of this work is to enlarge the confidence in current DOM transport models (such as those described in the literature (Put *et al.* 1998; Weetjens 2003; Maes *et al.* 2004; Ionescu *et al.* 2008; Martens *et al.* 2010; Durge *et al.* 2018) by (partial) validation). This is done by tweaking them to obtain the best possible fits to the experimental data of a unique long-term and large-scale *in situ* experiment with ^{14}C -labelled NOM, supplied to the Boom Clay from a horizontally and vertically inserted piezometer, which was set up in the framework of the TRANCOM-Clay project 25 years ago (Dierckx *et al.* 2000). This experiment is referred to as TDR41HV–TROM. The aim is to keep the model structure as parsimonious as possible by stepwise building the numerical flow and transport model and adding complexity (parameters and processes) at each step.

The TDR41HV–TROM in situ experiment: past and present

The large-scale *in situ* experiment, referenced to as TDR41HV–TROM, is performed in the **Test Drift** of the HADES URL, more particularly in **Ring 41** of the Test Drift, and concerns one horizontal (**H**) and one vertical (**V**) supporting tube (piezonest). Putting all the bold letters and numbers together leads to the name of the experiment: TDR41HV. TROM refers to the ^{14}C -labelled extracted DOM that is injected during the experiment. This paper concerns similar modelling efforts as performed in Martens *et al.* (2010). In that work, the authors gradually developed an axisymmetric model for the vertical piezometer by increasing the complexity of the model. First, only diffusion and linear sorption were included. In a subsequent step advection was added. Finally, the effect of adding a colloid transport model was evaluated. The final model was then validated on the dataset from the horizontal piezometer.

However, in the meantime the experiment has been continued for 12 more years, and data points

started to arise at the sampling points farther away from the injection point. Owing to increased computational resources, it was now possible to simultaneously fit concentrations at both the horizontal and vertical sampling filters around the URL using modern optimization algorithms. This allows more precise quantification of the influence of the Boom Clay anisotropy on the processes related to the migration of the organic species. Moreover, detailed hydraulic modelling of the drainage towards the gallery was included, which accurately represents the influence of advection on DOM transport. Most importantly, the influence of the different size fractions of the Boom Clay on transport are taken into account, which proved to be an essential aspect to in order describe the experimental data.

Materials and methods

Experimental setup: TDR41HV-TROM

The *in situ* experiment referred to as TDR41HV was described in detail in the literature (De Cannière *et al.* 1996; Dierckx *et al.* 2000; Maes *et al.* 2004; Van Laer 2018). Two piezometers installed in Ring 41

of the test gallery of the HADES URL in Mol (Fig. 1) and previously used to study iodide migration (De Cannière *et al.* 1996) were (re)used. One is oriented horizontally (migration parallel to the Boom Clay bedding) and the other is oriented vertically in the formation (migration perpendicular to the Boom Clay bedding as shown in Fig. 1). In each of these two piezometers nine porous stainless steel filters were placed at different distances. Each filter is equipped with tubing (in and out) allowing water circulation, either for tracer supply or for water sampling. A natural porewater solution (RBCW, Real Boom Clay Water; De Craen *et al.* 2004) containing ^{14}C -labelled extracted DOM is circulated every 4 h in the mixing chambers of injection filters R41-F8V and R41-F8H, in such a way that constant activity concentrations of 3.1×10^{10} and $2.2 \times 10^{10} \text{ Bq m}^{-3}$ solute are permanently maintained in the filter, for the vertical and horizontal piezometer, respectively. The total organic carbon values from the ^{14}C source solutions were 168 and 241 mgC l^{-1} for respectively R41-H and R41-V. Twice a year, water is collected (c. 100 ml) from the first two neighbouring filters, at a distance of respectively 0.35 and 0.85 m (filters R41-F7H, R41-F6H,

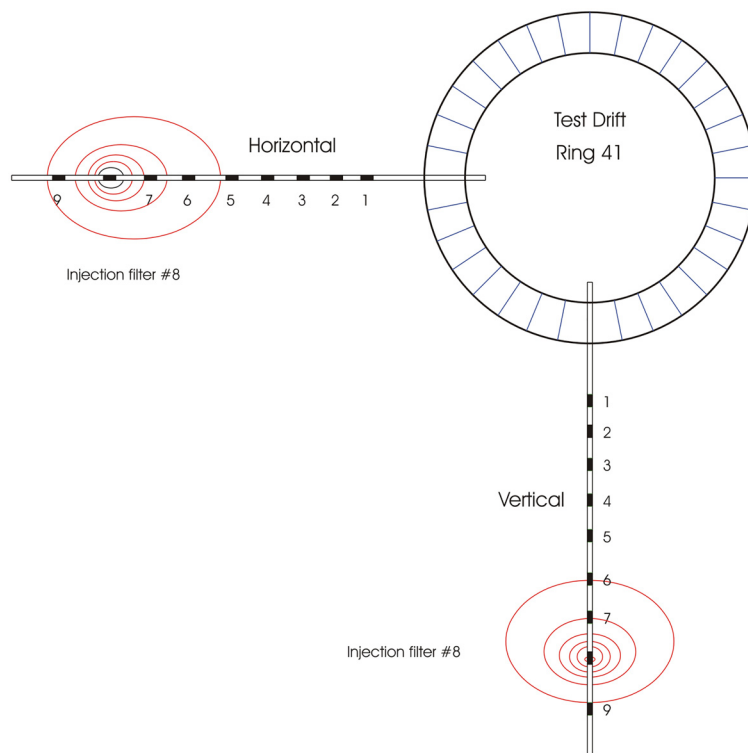


Fig. 1. Schematic representation of the emplacement of the horizontal (R41-H) and vertical (R41-V) piezometers in the HADES URL (SCK CEN, Mol, Belgium) for the migration experiment with ^{14}C -labelled natural organic matter.

R41-F7V and R41-F6V) and the ^{14}C activity is determined using liquid scintillation counting (LSC). A schematic drawing of the injection setup is given in the [Supplementary material](#).

^{14}C -labelled DOM solution

The ^{14}C -labelled DOM was prepared by Loughborough University in the framework of the EC TRANCOM-Clay Project using concentrated extracted Boom Clay organic matter. Details on the preparation and the experimental setup are given in [Dierckx *et al.* \(2000\)](#). In 2009, a size distribution analysis was performed on samples from the source solutions and the first neighbouring filters using filtration with ultrafiltration membranes of different molecular weight cut-off. Both the UV signal (as a measure of the organic matter content) and ^{14}C activity (using LSC) were measured.

Modelling approach

Mathematical model

For most radioactive solutes, transport through (saturated) Boom Clay can be well represented by the following classical conservation equation for advective–dispersive transport with linear reversible sorption in saturated porous media (adapted from [Fetter 1994](#)):

$$\begin{aligned} (\eta + \rho_b R_d) \frac{\partial c}{\partial t} - \nabla \cdot [\eta(D + D_p)\nabla c - \mathbf{u}_{\text{Darcy}}c] \\ = -\lambda(\eta + \rho_b R_d)c + S \end{aligned} \quad (1)$$

where c is the concentration of a given nuclide in the porewater (Bq m^{-3}), η is the (accessible) porosity, ρ_b is the dry bulk density (kg m^{-3}), R_d is the effective (solid/liquid) distribution coefficient ($\text{m}^3 \text{kg}^{-1}$), D is the hydrodynamic dispersion tensor ($\text{m}^2 \text{s}^{-1}$), D_p is the pore diffusion tensor ($\text{m}^2 \text{s}^{-1}$), $\mathbf{u}_{\text{Darcy}}$ is the Darcy velocity vector (m s^{-1}), λ is the radioactive decay rate (s^{-1}) and S is a generic reaction source term. In low permeability porous media, like Boom Clay, advection is usually small compared to diffusion and consequently dispersion terms are therefore negligible with regards to diffusion coefficients. The transport equation can then be simplified by dividing by η and the retardation factor (defined as $R = 1 + \rho_b R_d/\eta$) to

$$\frac{\partial c}{\partial t} - \nabla \cdot [D_{\text{app}}\nabla c - \mathbf{u}_{\text{app}}c] = -\lambda c + S^* \quad (2)$$

where D_{app} is the apparent diffusion tensor ($=D_p/R$) and \mathbf{u}_{app} is the apparent velocity vector according to

$$\mathbf{u}_{\text{app}} = \frac{\mathbf{u}_{\text{Darcy}}}{\eta R} \quad (3)$$

Transport of DOM is usually described with a classical advection–diffusion equation with linear sorption ([equation 1](#)). Reversible straining, filtration and/or sorption effects, which are typically observed in transport of colloidal species ([Sen and Khilar 2006](#); [Bradford *et al.* 2007](#); [Porubcan and Xu 2011](#)), are often lumped together into the effective solid/liquid distribution ratio (R_d) and as such the retardation factor. Owing to size (and charge) exclusion, not all species are probably able to access the entire pore space. When this inaccessible part of the total porosity contributes significantly to the total (Darcy) water flux through the clay, the value of \mathbf{u}_{app} might be significantly over- or underestimated as stated in [Aertsens *et al.* \(2020\)](#). However, this inaccessible pore fraction for (larger) particles most likely corresponds to zones of fluid stagnation while a few high velocity channels control the overall ability of the medium to transmit the fluid and contribute to the total water flow rate ([De Anna *et al.* 2017](#)). As such, this is not expected to introduce significant errors, especially in diffusion dominant systems.

To account for irreversible (immobilization) processes like physical entrapment, chemical irreversible sorption/attachment and/or dissociation of the ^{14}C -label, the reaction source term S^* can be used as a simple first-order decay term:

$$S^* = -\frac{\eta k_{\text{irr}}}{\eta R} c = -k_{\text{irr}}^* c \quad (4)$$

with k_{irr} and k_{irr}^* the lumped kinetic rate constants for all irreversible processes (s^{-1}). The term capacity factor is often used for the product of η and R .

Although the permeability of the Boom Clay is very low, advection cannot be neglected in this case owing to drainage towards the open gallery infrastructure of HADES. The Darcy velocity field is calculated from the steady state solution of Darcy's equation:

$$\mathbf{u}_{\text{Darcy}} = K_h \nabla H \quad (5)$$

where K_h is the hydraulic conductivity tensor (m s^{-1}) and H is the hydraulic head (m).

Model geometry, boundary conditions and parameters

Hydraulic model. In order to estimate the hydraulic effect of the presence of the HADES facility, a two-dimensional geometry of the experimental setup was modelled in COMSOL Multiphysics 5.6 ([COMSOL Multiphysics® 2020](#)). The URL gallery was represented as an open cylinder (with a radius of 1.75 m, at a depth of 225 m) at atmospheric

pressure in the centre of a Boom Clay volume of 25 by 25 m (by 1 m). Pressure heads at the boundaries are set to 200 and 250 m at respectively the top and bottom, with a linear interpolation between these values at the left and right sides (Fig. 2).

In a clay deposit such as the Boom Clay, low-porosity clay platelets are dominantly oriented perpendicular to the direction in which sedimentation took place, which becomes even more accentuated by compaction. Owing to this layered structure, hydraulic conductivities are higher in the direction parallel (//) than perpendicular (\perp) to the bedding plane. The best estimate values for the horizontal (//) and vertical (\perp) hydraulic conductivity the Boom Clay formation are 4.5×10^{-12} and $2.1 \times 10^{-12} \text{ m s}^{-1}$ respectively (Yu *et al.* 2013), which will be used in the hydraulic calculations.

Transport model. To model the evolution of the concentrations of DOM along the horizontal and vertical piezometers, two separate 2D axisymmetric models are constructed in COMSOL Multiphysics 5.6 (COMSOL Multiphysics® 2020). The geometry comprises the central part of the piezometer within a limited volume of Boom Clay (2 m radius \times 4 m height). The injection filter is modelled as a constant concentration boundary. All other boundaries are assigned no flux boundary conditions (Fig. 2).

Similar to the hydraulic conductivity, diffusion coefficients for solutes are usually higher in the

direction parallel (//) than perpendicular (\perp) to the bedding plane of Boom Clay. For instance, in the case of the non-sorbed tracer RN HTO, a value of 2 is considered as the best estimate for the ratio between the horizontal (//) and vertical (\perp) pore diffusion coefficients, although the anisotropy ratio can range between 1.5 and 3, depending on the degree of compaction (Bruggeman *et al.* 2009; Jacops *et al.* 2017).

The injected solution of ^{14}C -labelled DOM consisted of a complex mixture of organic molecules spanning a wide size distribution. As a consequence, to properly model the migration behaviour of the supplied DOM, more than one species having different migration parameters will probably have to be introduced, similar to Durce *et al.* (2018). Radioactive decay is neglected owing to the long half-life of ^{14}C (5730 years) in comparison to the duration of the experiment (*c.* 25 years).

Optimization. Different to the previous modelling of the *in situ* test in Martens *et al.* (2010), automated (global) optimization algorithms are applied (on data for all filters and in both directions). To avoid the best-fits being dominated by the high concentrations in the filters closest to the source filter, the sum of squared relative residuals (SSrR) between model and measurements was minimized using the MATLAB *lsqnonlin* and *multistart* functions (MATLAB

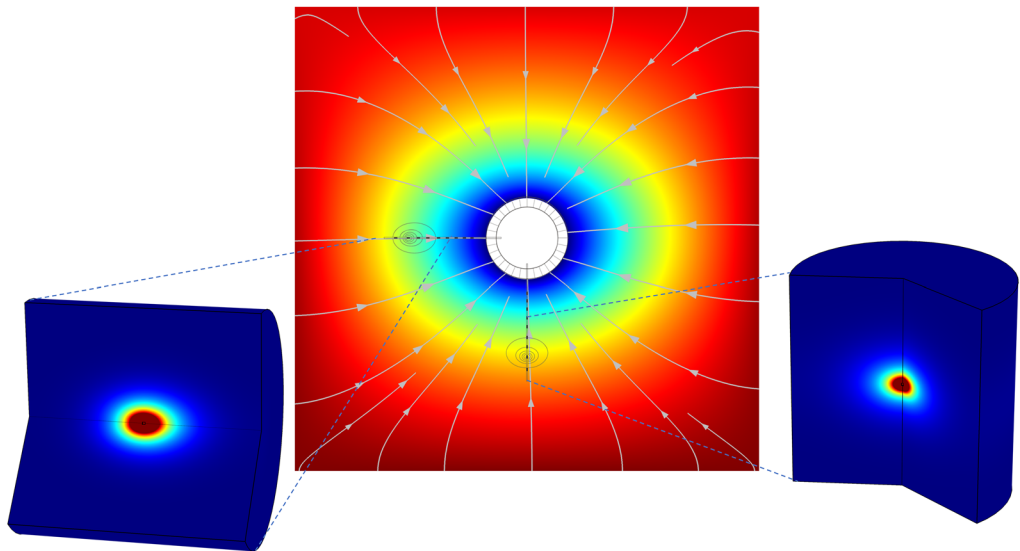


Fig. 2. Illustration of the setup of the numerical 2D cartesian hydraulic (centre, pressure head as surface plot and velocity distribution as arrow plot) and the two 2D axisymmetric transport models (for the horizontal and the vertical piezometer, respectively left and right, activity concentration evolution). Velocities along the piezometers are mapped from the steady-state solution of the hydraulic model to the transport models (these illustrations are not to scale and exaggerated parameter values are used for illustrative purposes).

2020). This SSrR is defined as:

$$\text{SSrR} = \sum_{j=1}^{N_f} \sum_{i=1}^{N_f} \left(\frac{c_i - c_{\text{exp},ij}}{c_{\text{exp},ij}} \right)^2 \quad (6)$$

with N the number of measurements for each filter, N_f the number of sampling filters, $c_{\text{exp},ij}$ the experimentally measured concentration and c_i the modelled concentration (being the sum of the concentrations of both modelled DOM species).

To judge the goodness-of-fit to the individual sampling filters, a coefficient of determination (R^2) is calculated based on the absolute differences (Witte and Witte 2017). One must keep in mind that this overemphasizes the importance of points with a high absolute value. A value closer to 1 indicates a better fit. The value of R^2 may be negative when a non-linear function is used to fit the data. In cases where negative values arise, the mean of the data provides a better fit to the measured data than the simulated values.

Results and discussion

Hydraulic model

Steady-state results from the hydraulic component of the model are shown in Figure 3. It is clear that the Darcy velocities and so the pressure gradients are higher closer to the gallery and smaller at larger distances from the gallery, which might have a (small) impact on the predictions of DOM breakthrough, compared with the fixed velocity which was used in previous modelling attempts of this experimental setup (Martens *et al.* 2010; Aertsens *et al.* 2013). Owing to the larger horizontal hydraulic conductivity, velocities are about two times higher along the

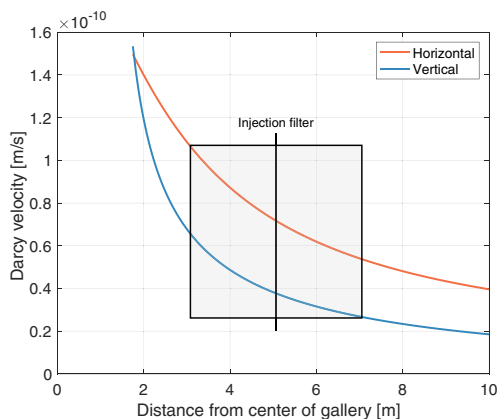


Fig. 3. Steady-state Darcy velocities around the open gallery.

horizontal piezometer. The calculated Darcy velocities along the piezometer (at 3–7 m from the centre of the gallery, corresponding to the length of the transport model domain) are transferred to the transport model, resulting in an imposed velocity field that is uniform in the radial direction and aligned with the axis along the piezometer.

DOM transport model

This section contains a description of the stepwise model building (Table 1), which will illustrate why and when more complexity (parameters and processes) is introduced into the model to better fit the data. By showing the minimized SSrR-value and coefficients of determination (R^2) for each filter, the goodness-of-fit of each successive model and its improvements are quantified. In every step, the data for all filters are simultaneously fitted by the optimization algorithm. Table 2 contains a description of the parameters that are used in the final model. In Table 3, optimal values for each fitting parameter and the 95% confidence intervals are given for each step of the model development. Please note that the R^2 for each sampling filter is based on absolute differences, while the SSrR is based on relative differences. As such, each data point will have an equal contribution to SSrR, while data points with a higher absolute value will have a higher weight in the individual R^2 values. Plots for each model fit are given in the Supplementary material, for completeness.

First, a simple isotropic diffusion model with one species is used to simulate the data in all four sampling locations (step 0, **Model_Di**). As expected, this model – with one fitting parameter D_{app} – does not succeed in providing a good fit to any of the datasets. Attempts to optimize the fit to one sampling location, either on the horizontal or vertical piezometer, consistently result in very poor fits to all others.

A reasonable fit at the closest filters (35 cm, F7H/V) leads to a strong underestimation of the concentrations at the farthest filters, while a reasonable fit at the farthest filters at 85 cm from the injection point (F6H/V) results in a strong over-prediction of concentrations in filters F7H/V. It appears clearly that the anisotropy of the Boom Clay plays a significant role as any value of the ^{14}C -DOM diffusion coefficient is unable to fit either the combination F7H/F7V or F6H/F6V.

Owing to the layered structure, Boom Clay shows anisotropy for hydraulic conductivity and diffusivity with both parameters higher in the direction parallel (//) than perpendicular (⊥) to the bedding plane. Pore throat orientation analyses on pore networks extracted from X-ray m-CT and FIB-SEM, performed in Hemes *et al.* (2015), show a strong anisotropy of the pore space connectivity, with

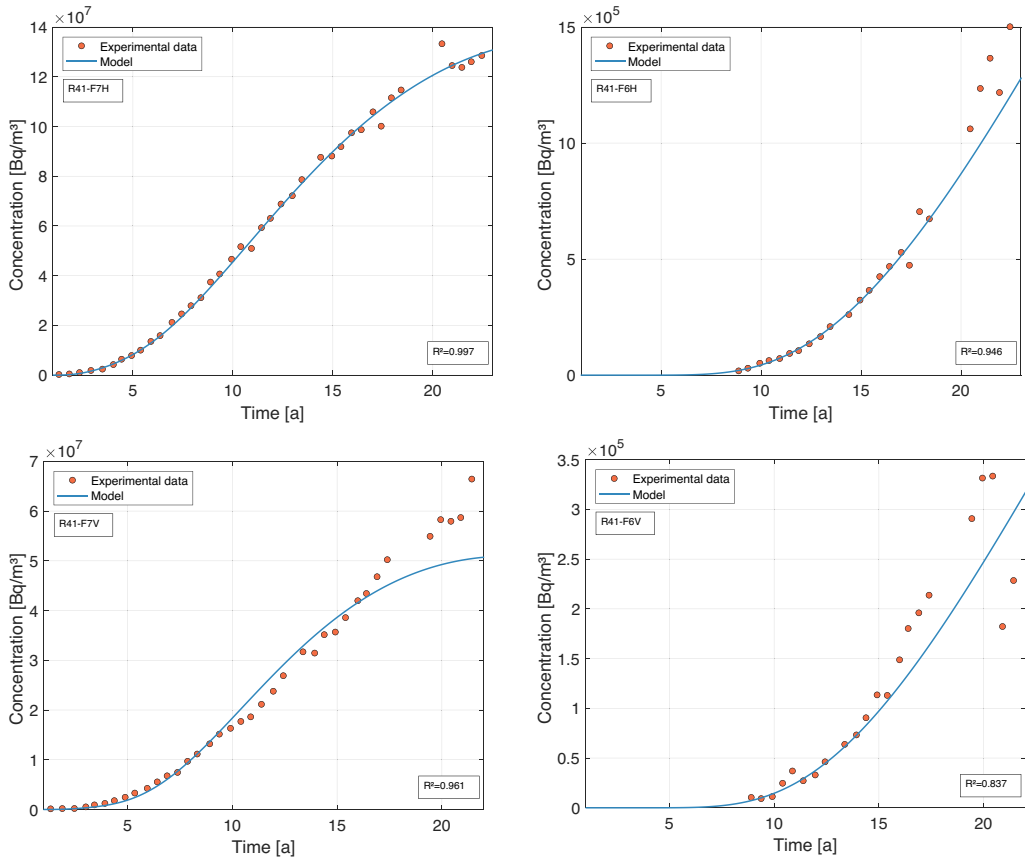


Fig. 4. Experimental data and optimal model fit at the horizontal piezometer – filters R41-F7H and R41-F6H (top, respectively 0.35 and 0.85 m from the injection filter) – and vertical piezometer – filters R41-F7V and R41-F6V (bottom, respectively 0.35 and 0.85 m from the injection filter).

Table 1. Description of the different steps in the stepwise model building

Step	Model name	Description	Number of fitting parameters
0	Model_Di	Isotropic diffusion using one species, no advection	1
1	Model_D1	Anisotropic diffusion using one species, no advection	2
2	Model_D2	Anisotropic diffusion using two species, no advection	6
3	Model_AD2	Anisotropic diffusion using two species, advection	8
4	Model_AD2_cap2	Anisotropic diffusion using two species, advection, different capacity factors used in the vertical and horizontal piezometer setup	8
5	Model_AD2_cap2_imm	Anisotropic diffusion using two species, advection, different capacity factors used in the vertical and horizontal piezometer setup, immobilization of the <i>slow</i> species	9
6	Model_AD2_cap2_imm2	Anisotropic diffusion using two species, advection, specific capacity factors for the vertical and horizontal piezometer setup, specific immobilization of the <i>slow</i> species for the vertical and horizontal piezometer setup	10

Table 2. Parameters that are used in the final model and their description

Parameter	Description
$D_{app_v_fast}$	Apparent diffusion coefficient of the 'fast' species in the vertical direction ($m^2 s^{-1}$)
$D_{app_h_fast}$	Apparent diffusion coefficient of the 'fast' species in the horizontal direction ($m^2 s^{-1}$)
$D_{app_v_slow}$	Apparent diffusion coefficient of the 'slow' species in the vertical direction ($m^2 s^{-1}$)
$D_{app_h_slow}$	Apparent diffusion coefficient of the 'slow' species in the horizontal direction ($m^2 s^{-1}$)
Fraction _{VP_slow}	Fraction of the 'slow' species in the source solution of the vertical piezometer relative to the total amount (—)
Fraction _{HP_slow}	Fraction of the 'slow' species in the source solution of the horizontal piezometer relative to the total amount (—)
ηR_{VP_fast}	Capacity factor of the 'fast' species for the vertical piezometer setup (—)
ηR_{HP_fast}	Capacity factor of the 'fast' species for the horizontal piezometer setup (—)
ηR_{slow}	Capacity factor of the 'slow' species (—)
$k_{irr_VP_slow}^*$	Effective kinetic rate of the 'slow' species for the vertical piezometer setup (s^{-1})
$k_{irr_HP_slow}^*$	Effective kinetic rate of the 'slow' species for the horizontal piezometer setup (s^{-1})

preferred pore throat orientations parallel to the sample bedding. This orientation corresponds to the horizontal direction in this work. Similar findings resulted from research using TEM and FIB/SEM imaging on Callovo-Oxfordian Clay, where the authors noticed clay particles mainly oriented perpendicular to the compaction axis and pores elongated in the same plane (Gaboreau *et al.* 2016).

The anisotropy of Boom Clay is therefore taken into account in the next modelling step by fitting the diagonal coefficients of the diffusion tensor, with a horizontal ($D_{app,h} = D_{xx} = D_{yy}$) and a vertical component ($D_{app,v} = D_{zz}$) while still considering only one ^{14}C -DOM species (**Model_D1**). This results in a significant improvement of the fits of the nearest filters (F7H/F7V) with R^2 -values rising to 0.6. However, the concentration values at the farthest filters are still largely underestimated. This could indicate that a small part of the injected DOM migrates faster than the rest and is able to travel farther and reach the F6H/F6V filters. So in a next step, the migration behaviour of the organic mixture is modelled using two species with distinct diffusion parameters, one 'fast' and one 'slow' (**Model_D2**). The ratio between the concentration of the slow species and the total concentration in the inlet filter is fitted separately for the vertical and horizontal piezometer and is denoted by respectively Fraction_{VP_slow} and Fraction_{HP_slow}. These are defined as:

$$\text{Fraction}_{slow} = \frac{c_{slow,inlet}}{c_{total,inlet}} \quad (7)$$

with $c_{slow,inlet}$ as the activity concentration of the slow species, and $c_{total,inlet}$ as the total activity concentration in the injection filter, which differs for the horizontal and the vertical piezometer.

These parameters are empirical fitting factors that are not linked to the actual DOM size distribution.

By introducing the additional fast component, overall fit quality improves drastically as seen by the large drop of the objective function value and increased R^2 -values in all four sampling filters.

However, a significantly lower Fraction_{HP_slow} compared with Fraction_{VP_slow} is obtained. It appears that along the horizontal piezometer setup, a larger part of the injected DOM population is able to migrate rather fast than slow and reach the farthest filter F6H. This can be attributed to the anisotropy of the pore connectivity and pore throat orientation/size. In the vertical direction, the pore throat diameter is smaller, resulting in a smaller fraction of molecules that are small enough to take the shortest possible pathway towards filter F6V.

The next process considered is advection. Owing to the drainage towards the open gallery infrastructure of HADES, advection is present and its role in the DOM transport is evaluated by adding it into the model. Velocity profiles obtained from the hydraulic calculation are mapped to the axisymmetric transport models (**Model_AD2**). This introduces two more fitting parameters: the capacity factors for the fast and the slow species $\eta R_{fast}/\eta R_{slow}$ which act as a scaling factor to the Darcy velocity, as seen in equation (3). Only a slight increase in overall fit quality is obtained, mostly in the farthest filter, indicating that the contribution of advection to the total transport must be small. Moreover, as indicated by the rather large fitted value (and also associated uncertainty) of ηR_{slow} , the *slow* species is even hardly transported by advection at all, compared with its diffusive counterpart. Larger particles are more prone to sorb on mineral surfaces and/or straining in too small pores and are therefore barely travelling along with the water flow, hence the low apparent velocity u_{app} . Because of the very low sensitivity of the model to the ηR_{slow} parameter, in the next model steps, it is fixed to a value of 4.

Table 3. Optimal and fixed parameter values and associated 95% confidence intervals for each step of the model development, SSrR and R²-values for all four sampling filters

Step 0: Model_Di													R ²	R ²	R ²	R ²	SSrR
	D _{app} (m ² s ⁻¹)	/	/	/	/	/	/	/	/	/	/	/	F7V	F6V	F7H	F6H	
Best fit	2.06 × 10 ⁻¹¹												0.052	-1.465	0.302	-1.105	88.419
±	1.80 × 10 ⁻¹²																
Step 1: Model_D1													R ²	R ²	R ²	R ²	SSrR
	D _{app,v} (m ² s ⁻¹)	D _{app,h} (m ² s ⁻¹)	/	/	/	/	/	/	/	/	/	/	F7V	F6V	F7H	F6H	
Best fit	2.04 × 10 ⁻¹¹	3.03 × 10 ⁻¹¹											0.589	-1.467	0.603	-0.989	73.804
±	1.84 × 10 ⁻¹²	2.97 × 10 ⁻¹²															
Step 2: Model_D2													R ²	R ²	R ²	R ²	SSrR
	D _{app,v,fast} (m ² s ⁻¹)	D _{app,h,fast} (m ² s ⁻¹)	D _{app,v,slow} (m ² s ⁻¹)	D _{app,h,slow} (m ² s ⁻¹)	Fraction _{VP,slow} (—)	Fraction _{HP,slow} (—)	/	/	/	/	/	/	F7V	F6V	F7H	F6H	
Best fit	9.18 × 10 ⁻¹¹	9.60 × 10 ⁻¹¹	1.77 × 10 ⁻¹¹	2.41 × 10 ⁻¹¹	0.984	0.929							0.877	0.783	0.944	0.952	10.958
±	7.92 × 10 ⁻¹²	6.95 × 10 ⁻¹²	9.84 × 10 ⁻¹³	1.95 × 10 ⁻¹²	0.006	0.023											
Step 3: Model_AD2													R ²	R ²	R ²	R ²	SSrR
	D _{app,v,fast} (m ² s ⁻¹)	D _{app,h,fast} (m ² s ⁻¹)	D _{app,v,slow} (m ² s ⁻¹)	D _{app,h,slow} (m ² s ⁻¹)	Fraction _{VP,slow} (—)	Fraction _{HP,slow} (—)	η _{R,fast} (—)	η _{R,slow} (—)	/	/	/	/	F7V	F6V	F7H	F6H	
Best fit	8.89 × 10 ⁻¹¹	9.08 × 10 ⁻¹¹	1.70 × 10 ⁻¹¹	2.28 × 10 ⁻¹¹	0.985	0.935	0.887	3.999					0.867	0.808	0.922	0.984	10.909
±	7.84 × 10 ⁻¹²	7.77 × 10 ⁻¹²	2.92 × 10 ⁻¹²	6.40 × 10 ⁻¹²	0.006	0.025	0.545	3.963									
Step 4: Model_AD2_cap2													R ²	R ²	R ²	R ²	SSrR
	D _{app,v,fast} (m ² s ⁻¹)	D _{app,h,fast} (m ² s ⁻¹)	D _{app,v,slow} (m ² s ⁻¹)	D _{app,h,slow} (m ² s ⁻¹)	Fraction _{VP,slow} (—)	Fraction _{HP,slow} (—)	η _{R,VP,fast} (—)	η _{R,HP,fast} (—)	/	/	/	/	F7V	F6V	F7H	F6H	
Best fit	8.77 × 10 ⁻¹¹	9.03 × 10 ⁻¹¹	1.72 × 10 ⁻¹¹	2.29 × 10 ⁻¹¹	0.988	0.937	0.309	0.800					0.847	0.791	0.920	0.984	10.508
±	7.75 × 10 ⁻¹²	7.71 × 10 ⁻¹²	9.25 × 10 ⁻¹³	1.86 × 10 ⁻¹²	0.005	0.023	0.200	0.502									
Step 5: Model_AD2_cap2_imm													R ²	R ²	R ²	R ²	SSrR
	D _{app,v,fast} (m ² s ⁻¹)	D _{app,h,fast} (m ² s ⁻¹)	D _{app,v,slow} (m ² s ⁻¹)	D _{app,h,slow} (m ² s ⁻¹)	Fraction _{VP,slow} (—)	Fraction _{HP,slow} (—)	η _{R,VP,fast} (—)	η _{R,HP,fast} (—)	k [*] _{irr,slow} (s ⁻¹)	/	/	/	F7V	F6V	F7H	F6H	
Best fit	9.94 × 10 ⁻¹¹	9.76 × 10 ⁻¹¹	2.47 × 10 ⁻¹¹	3.33 × 10 ⁻¹¹	0.994	0.955	0.194	0.796	2.22 × 10 ⁻⁹				0.988	0.839	0.963	0.953	6.885
±	8.47 × 10 ⁻¹²	7.76 × 10 ⁻¹²	1.68 × 10 ⁻¹²	3.33 × 10 ⁻¹²	0.002	0.022	0.090	0.536	5.13 × 10 ⁻¹⁰								
Step 6: Model_AD2_cap2_imm2													R ²	R ²	R ²	R ²	SSrR
	D _{app,v,fast} (m ² s ⁻¹)	D _{app,h,fast} (m ² s ⁻¹)	D _{app,v,slow} (m ² s ⁻¹)	D _{app,h,slow} (m ² s ⁻¹)	Fraction _{VP,slow} (—)	Fraction _{HP,slow} (—)	η _{R,VP,fast} (—)	η _{R,HP,fast} (—)	k [*] _{irr,VP,slow} (s ⁻¹)	k [*] _{irr,HP,slow} (s ⁻¹)	/	/	F7V	F6V	F7H	F6H	
Best fit	1.02 × 10 ⁻¹⁰	9.81 × 10 ⁻¹¹	2.67 × 10 ⁻¹¹	2.99 × 10 ⁻¹¹	0.995	0.945	0.170	0.799	3.15 × 10 ⁻⁹	1.26 × 10 ⁻⁹			0.961	0.837	0.997	0.945	6.288
±	8.64 × 10 ⁻¹²	7.23 × 10 ⁻¹²	1.85 × 10 ⁻¹²	3.87 × 10 ⁻¹²	0.002	0.022	0.075	0.511	7.06 × 10 ⁻¹⁰	8.32 × 10 ⁻¹⁰							
Fixed parameters																	
Hydraulic conductivity (horizontal)	4.5 × 10 ⁻¹² m s ⁻¹																
Hydraulic conductivity (vertical)	2.1 × 10 ⁻¹² m s ⁻¹																
Bulk density Boom Clay	1700 kg m ⁻³																

It can be reasonably expected that colloidal particles will show a different transport behaviour when the dominant direction of the water flow is parallel or perpendicular to the bedding planes of the clay. When concentrations in the horizontal sampling filters (R41-7H and R41-6H) are modelled, the main transport and water flow direction is along the bedding. As such, the particles are able to move through larger pores that show better connectivity. This effect is enhanced by a higher water velocity in the horizontal direction towards the gallery compared to the vertical direction (Fig. 3). This forces particles preferentially into the larger pores of the pore size distribution (Sirivithayapakorn and Keller 2003). Therefore, particles travelling along the horizontal piezometer will be able to enter a larger fraction of the total porosity (η), often referred to as the accessible porosity.

On the other hand, owing to the higher horizontal water velocities, when particles eventually end up being strained in narrow pores, it is harder to diffuse out. This effect enhances retardation (R) and altogether leads to a higher capacity factor ηR of the fast compounds for the transport along the horizontal piezometer compared with the vertical piezometer. This is confirmed by fitting different capacity factors for each piezometer setup (**Model_AD2_cap2**). The objective function value drops significantly while individual R^2 values decrease slightly. This means that early breakthrough points are fitted better at the expense of later data points with higher concentration values. The capacity factor fitted for the horizontal piezometer setup is found to be about 2.5 times higher compared with the vertical piezometer.

Concentrations at the F7H/F7V filters appear to be levelling off after 15 years of data collection (Fig. 4). However, the diffusion model predicts a steep rise of the concentrations (see **Model_AD2** in the [Supplementary material](#)), which should eventually reach the level of the inlet filter concentrations once a (pseudo-)steady state is reached. This indicates that a significant fraction of the 'slow' injected DOM is not able to migrate and will be immobilized along the way towards the sampling points. By adding a first-order kinetic term to the model of the slow compounds, irreversible immobilization (equation 4) is introduced: first by using one constant for both horizontal and vertical piezometers (**Model_AD2_cap2_imm**), then by using a specific one for each piezometer (**Model_AD2_cap2_imm2**). Kinetic rate constants are only fitted for the slow compounds, as they are not identifiable for the fast compounds while the concentration data in the F6 filters is still rising and not nearing a plateau. Moreover, the fast compounds are not expected to get immobilized. Adding the kinetic terms greatly improves model fit quality, as can

be seen in Table 3. By fitting different kinetics for the vertical and horizontal piezometer, fit quality improves even more (final **Model_AD2_cap2_imm2**, Fig. 4). The lower connectivity and smaller pore size in the vertical direction result in a more efficient filtering and irreversible entrapment of the larger DOM molecules when water flow is perpendicular to the bedding plane, leading to a larger kinetic constant for the vertical piezometer. By introducing the kinetic term, the diffusion coefficient values increased slightly in order to compensate for part of the immobilized fraction.

Size distribution

In 2009 (Martens *et al.* 2010), size distribution analysis was performed on samples from the source solutions and the first neighbouring filters using filtration with ultrafiltration membranes of different molecular weight cut-off. Both the UV signal (as a measure of the organic matter content) and ^{14}C activity (using LSC) were measured. Later on, a new sample from the source solution of the horizontal source filter (F8H) was analysed to determine the size distribution using the more accurate HPLC–SEC technique (Durce *et al.* 2017). These recent measurements confirmed the earlier results and they show that the major size fractions of the mobile organic matter were the ones below 1 kDa and between 1 and 10 kDa, together with the presence of small fractions of larger molecules (Fig. 5).

As the distributions of the source solutions show the same features, the ^{14}C label was homogeneously distributed over the complete DOM pool. Further on, an enrichment of the smaller size molecules in the sampling filters F7V/F7H was observed with respect to the source solutions, which indicates the inability of the larger molecules to diffuse through the Boom Clay that appears to act like a molecular filter. The enrichment of the smallest molecules is less pronounced in the horizontal piezometer setup. This confirms the modelling results in which a larger fast fraction is obtained for the HP, together with smaller immobilization kinetics.

Discussion on the final model

Stepwise addition of more complexity (parameters and processes) to the DOM transport eventually resulted in a model with 10 fitting (and one fixed) parameters with which excellent fits are obtained to the *in situ* experiment. No strong correlations between these parameters are identified, as indicated by the unique, global solution to the optimization and the relatively narrow confidence intervals on the corresponding optimal values. The final model

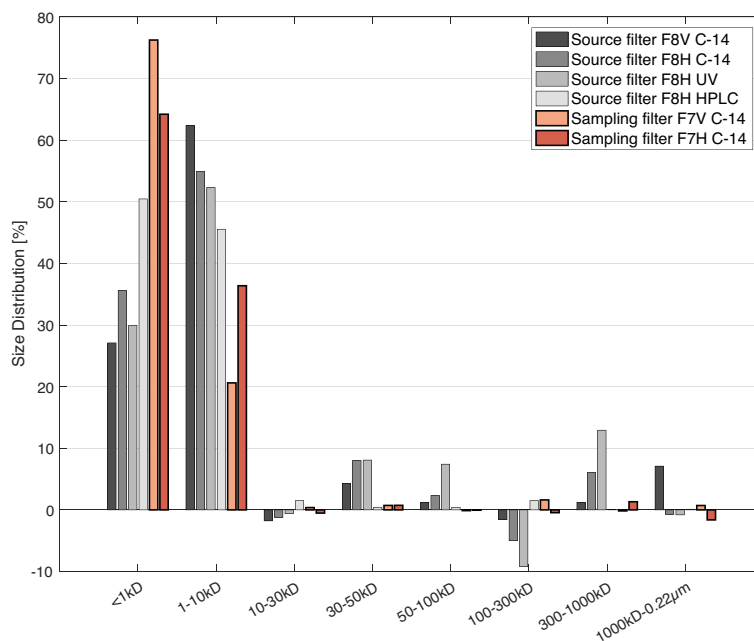


Fig. 5. DOM size distribution of the solutions obtained from source filters (F8V/F8H) and sampling filters (F7H/F7V), based on the measurement of ^{14}C -activity and UV-absorbance on ultra-filtrated samples and using HPLC-SEC.

is a straightforward one using the classical advection–diffusion equation for two different classes of DOM, a slow and a fast one, similar to work in the literature (Weetjens 2003; Maes *et al.* 2004), where two different classes with different retardation factors were used to describe lab-scale experiments under *in situ* conditions. The relative amounts of fast/slow compounds are empirical fitting factors and are not directly derivable from molecular size distributions. However, it is clear that molecular size plays a primordial role in the distinction between a fast and a slow compound, as also noted by Durce *et al.* (2018), who derived size-dependent migration parameters for the whole organic matter size spectrum. Finally, a kinetic term is added to account for irreversible immobilization of the larger subgroup of the slow compounds. Therefore, the resulting model is strongly in line with previously derived models (Maes *et al.* 2004; Hicks 2008; Ionescu *et al.* 2008; Martens *et al.* 2010; Durce *et al.* 2018) which combine classical advection–diffusion equations with kinetic attachment/immobilization terms.

Generally, models with many parameters (and non-linear interactions) require a lot of good-quality data to constrain their parameters during calibration. Model complexity and the number and information content of experimental data should be well balanced. If the model contains too many

parameters for the given number of data, it might show a good fit during calibration, but a high variance (i.e. the error owing to sensitivity to noise in the data) and the ability of the model to generalize beyond the available experiments is reduced. This effect is known as overfitting. On the other hand, a model that is too simple needs less data for calibration but shows a high systematic bias between its predictions and measured data and thus ‘underfits’ the system (Lever *et al.* 2016). For instance, the first *c.* 15 years of the experimental data do not allow the immobilization kinetics to be constrained, but can be well described by a simpler variant of the model, as shown in Van Laer (2018). However, this model would fail to predict correct concentrations of the last 7–10 years of the experiment, emphasizing the value of continuing *in situ* experiments for a sufficient amount of time. By doing this, a high-quality dataset was obtained which allowed the accurate calibration of a numerical model for the complex migration behaviour of DOM, without over- or underfitting.

When upscaling the model to the level of the host rock scale for safety and performance assessment purposes, one must keep in mind that the dominant transport mode is diffusion and the main direction of interest is vertically (upwards and downwards through the Boom Clay towards the surrounding aquifers). This makes the apparent vertical

diffusion coefficient the most relevant parameter. The values of the vertical apparent diffusion coefficient of the fast compound ($1.02 \pm 0.09 \times 10^{-10} \text{ m}^2 \text{ s}^{-1}$) are close to the high end of the range reported for the most mobile DOM classes in Bruggeman and Maes (2017) and Durce *et al.* (2018). Bruggeman and Maes (2017) suggested $8.9 \times 10^{-11} \text{ m}^2 \text{ s}^{-1}$ for Boom Clay DOM <1 kDa and Durce *et al.* (2018) suggested $7.5 \times 10^{-11} \text{ m}^2 \text{ s}^{-1}$ for species with $\log(\text{MW}) < 3.3$. The fact that the values in the current work are even higher is because they probably belong to a very mobile subgroup of those classes: the ones that are able to diffuse through 85 cm of clay in significant quantities. This also explains the low fraction of these mobile, fast molecules. The same authors report values for less or partly mobile Boom Clay DOM: ranging from 0.5×10^{-11} to $1.0 \times 10^{-11} \text{ m}^2 \text{ s}^{-1}$ (from Bruggeman and Maes (2017) for >1 kDa) and from 1×10^{-11} to $3.2 \times 10^{-11} \text{ m}^2 \text{ s}^{-1}$ (from Durce *et al.* (2018) for $3.3 < \log(\text{MW}) < 4$). The value obtained for the slow compound is in the same range albeit again at the higher end ($2.67 \pm 0.19 \times 10^{-11} \text{ m}^2 \text{ s}^{-1}$). So, diffusion coefficients obtained from the best-fit of the *in situ* experiment (metre-scale) compare quite well with those obtained from lab-scale experiments (centimetre-scale). This means that models based on lab-scale experiments allow a good approximation to be made of the transport on larger scales when diffusion is the dominant mechanism, as it is in the TDR41HV–TROM experiment and as it is expected on host rock scale. This adds confidence to the DOM modelling performed within the context of a safety assessment.

Care must be taken when irreversible immobilization kinetics are applied in an upscaled PA/SA-type model. Processes that seem irreversible on the timescale of the *in situ* experiment (*c.* 25 years) might not be on the timescale of a safety assessment (more than thousands of years). Also, some immobilization processes might be enhanced by the pressure difference induced by the drainage towards the HADES URL which is not expected during long-term operation of the underground disposal facility. It would be advisable to conservatively neglect these irreversible processes.

Conclusions

An *in situ* migration experiment with ^{14}C -labelled DOM was performed at the HADES URL to study its migration behaviour at the metre scale, different orientations with respect to the bedding plane and on a time scale of 25 years.

Stepwise addition of more complexity (parameters and processes) to the DOM transport eventually resulted in a model with 10 fitting parameters with

which excellent fits are obtained to the *in situ* experimental results. The model considers two different fractions, one that migrates fast and one that migrates slowly, which are transported by advection and diffusion and can be subject to both irreversible as reversible immobilization and retardation processes. All of these processes are strongly influenced by the anisotropy of the pore structure of the Boom Clay.

The dominant process is diffusion and its associated fitted parameter values compare well with values determined on small-scale migration experiments. Similar to the findings of Durce *et al.* (2018), it was key to explicitly model the migration of species with different migration behaviours, subject to irreversible immobilization. This builds confidence in the DOM transport model and its associated parameter values, which in turn contributes to the confidence in the outcome of the RN migration calculations performed in the context of a safety and performance assessment.

Acknowledgements The authors would like to express their appreciation to all colleagues who have contributed over the past 40 years to long-term *in situ* experiments such as the one discussed in this paper.

Competing interests The authors declare that they have no known competing financial interests or personal relationships that could have appeared to influence the work reported in this paper, except from the agencies to which the authors are affiliated.

Author contributions JG: formal analysis (lead), investigation (lead), software (lead), writing – original draft (lead); NM: data curation (lead), methodology (supporting), writing – review & editing (lead); DD: writing – review & editing (supporting); MA: writing – review & editing (equal); SB: resources (lead), writing – review & editing (supporting).

Funding This research received no specific grant from any funding agency in the public, commercial or not-for-profit sectors.

Data availability The data that support the findings of this study are available from EIG EURIDICE, SCK CEN and NIRAS/ONDRAF but restrictions apply to the availability of these data, which were used under licence for the current study, and so are not publicly available. Data are, however, available from the authors upon reasonable request and with permission of EIG EURIDICE, SCK CEN and NIRAS/ONDRAF.

References

- Aertsens, M., Maes, N., Van Ravestyn, L. and Brassinnes, S. 2013. Overview of radionuclide migration experiments in the HADES underground research facility at

- Mol (Belgium). *Clay Minerals*, **48**, 153–166, <https://doi.org/10.1180/claymin.2013.048.2.01>
- Aertsens, M., Maes, N., Govaerts, J. and Durce, D. 2020. Why tracer migration experiments with a pressure gradient do not always allow a correct estimation of the accessible porosity in clays. *Applied Geochemistry*, **120**, 104672, <https://doi.org/10.1016/j.apgeochem.2020.104672>
- Bradford, S.A., Torkzaban, S. and Walker, S.L. 2007. Coupling of physical and chemical mechanisms of colloid straining in saturated porous media. *Water Research*, **41**, 3012–3024, <https://doi.org/10.1016/J.WATRES.2007.03.030>
- Bruggeman, C. and De Craen, M. 2012. Boom Clay natural organic matter – Status Report 2011, **SCKCEN-ER-206**, <https://researchportal.sckcen.be/en/publications/boom-clay-natural-organic-matter-status-report-2011>
- Bruggeman, C. and Maes, N. 2017. Radionuclide migration and retention in Boom Clay, **SCKCEN-ER-0345**, <https://researchportal.sckcen.be/en/publications/radionuclide-migration-and-retention-in-boom-clay>
- Bruggeman, C., Maes, N., Aertsens, M. and De Cannière, P. 2009. Tritiated water retention and migration behaviour in Boom Clay. SFC1 Level 5 Report: First Full Draft, **SCKCEN-ER-248**, <https://researchportal.sckcen.be/en/publications/tritiated-water-retention-and-migration-behaviour-in-boom-clay-sf>
- Bruggeman, C., Liu, D.J. and Maes, N. 2010. Influence of Boom Clay organic matter on the adsorption of Eu^{3+} by illite-geochemical modelling using the component additivity approach. *Radiochimica Acta*, **98**, <https://doi.org/10.1524/ract.2010.1759>
- Bruggeman, C., Salah, S., Maes, N. and Durce, D. 2017a. Americium retention and migration behaviour in Boom Clay: Topical report – status 2015, **SCKCEN-ER-0396**. SCK•CEN Reports, <https://researchportal.sckcen.be/en/publications/amerium-retention-and-migration-behaviour-in-boom-clay-topical>
- Bruggeman, C., Maes, N. *et al.* 2017b. Technetium retention and migration behaviour in Boom Clay: Topical report – status 2015, **SCKCEN-ER-0403**. SCK•CEN Reports, <https://researchportal.sckcen.be/en/publications/technetium-retention-and-migration-behaviour-in-boom-clay-topical>
- COMSOL Multiphysics® 2020. Version 5.6, <https://www.comsol.com/>
- De Anna, P., Quaipe, B., Biros, G. and Juanes, R. 2017. Prediction of the low-velocity distribution from the pore structure in simple porous media. *Physical Review Fluids*, **2**, 1–16, <https://doi.org/10.1103/PhysRevFluids.2.124103>
- De Cannière, P., Moors, H., Lolivier, P., De Preter, P. and Put, M. 1996. Laboratory and *in situ* migration experiments in the Boom Clay. European Commission Nuclear Science and Technology Report, **EUR 16927 EN**.
- De Craen, M., Wang, L., Van Geet, M. and Moors, H. 2004. Geochemistry of Boom Clay pore water at the Mol site, **SCKCEN-BLG-990**, <https://researchportal.sckcen.be/en/publications/geochemistry-of-boom-clay-pore-water-at-the-mol-site-status-2004>
- Dierckx, A., Maes, A. and Vancluyse, J. 1994. Mixed complex formation of Eu^{3+} with humic acid and a competing ligand. *Radiochimica Acta*, **66–67**, 149–156, <https://doi.org/10.1524/RACT.1994.6667.SPECIAL-ISSUE.149>
- Dierckx, A., Put, M. *et al.* 2000. Transport of radionuclides due to complexation with organic matter in clay formations – Trancom-Clay, European Commission Nuclear Science and Technology Final Report, **EUR 19135**.
- Durce, D., Bruggeman, C., Maes, N., Van Ravestyn, L. and Brabants, G. 2015. Partitioning of organic matter in Boom Clay: leachable vs mobile organic matter. *Applied Geochemistry*, **63**, 169–181, <https://doi.org/10.1016/J.APGEOCHEM.2015.08.009>
- Durce, D., Aertsens, M., Bruggeman, C., Maes, N., Salah, S., Van Laer, L. and Van Gompel, M. 2017. Water-soluble organic matter in Boom Clay. Status report 2012–2016, **SCK CEN ER-0382**, <https://researchportal.sckcen.be/en/publications/water-soluble-organic-matter-in-boom-clay-status-report-2012-2016>
- Durce, D., Aertsens, M., Jacques, D., Maes, N. and Van Gompel, M. 2018. Transport of dissolved organic matter in Boom Clay: Size effects. *Journal of Contaminant Hydrology*, **208**, 27–34, <https://doi.org/10.1016/j.jconhyd.2017.12.004>
- Fetter, C. 1994. *Applied Hydrogeology*. 3rd edn. Waveland Press.
- Gaboreau, S., Robinet, J.C. and Prêt, D. 2016. Optimization of pore-network characterization of a compacted clay material by TEM and FIB/SEM imaging. *Microporous and Mesoporous Materials*, **224**, 116–128, <https://doi.org/10.1016/j.micromeso.2015.11.035>
- Govaerts, J. and Weetjens, E. 2017. Applying the principles of verification, qualification and validation to computer codes used in the long-term safety assessments for geological disposal of B&C waste, **SCK CEN I-0550**.
- Hemes, S., Desbois, G., Urai, J.L., Schröppel, B. and Schwarz, J.O. 2015. Multi-scale characterization of porosity in Boom Clay (HADES-level, Mol, Belgium) using a combination of X-ray $\mu\text{-CT}$, 2D BIB-SEM and FIB-SEM tomography. *Microporous and Mesoporous Materials*, **208**, 1–20, <https://doi.org/10.1016/j.micromeso.2015.01.022>
- Hicks, T. 2008. POPCORN modelling of migration experiments to investigate the effects of organic matter on radionuclide transport in the Boom Clay.
- IAEA 2019. *Safety Glossary*. 2018 edition, <https://www.iaea.org/publications/11098/iaea-safety-glossary-2018-edition>
- Ionescu, A., Maes, N. and Mallants, D. 2008. Modelling transport of ^{14}C -labelled natural organic matter (NOM) in Boom Clay. *Materials Research Society Symposium Proceedings*, **1107**, 629–636, <https://doi.org/10.1557/PROC-1107-629>
- Jacops, E., Aertsens, M. *et al.* 2017. Interplay of molecular size and pore network geometry on the diffusion of dissolved gases and HTO in Boom Clay. *Applied Geochemistry*, **76**, 182–195, <https://doi.org/10.1016/j.apgeochem.2016.11.022>
- Lever, J., Krzywinski, M. and Altman, N. 2016. Points of significance: model selection and overfitting. *Nature Methods*, **13**, 703–704, <https://doi.org/10.1038/nmeth.3968>
- Liu, D.J., Bruggeman, C. and Maes, N. 2008. The influence of natural organic matter on the speciation and

- solubility of Eu in Boom Clay porewater. *Radiochimica Acta*, **96**, <https://doi.org/10.1524/ract.2008.1557>
- Maes, A., Bruggeman, C., Geraedts, K. and Vancluyse, J. 2003. Quantification of the interaction of Tc with dissolved Boom Clay humic substances. *Environmental Science and Technology*, **37**, <https://doi.org/10.1021/es020091v>
- Maes, N., Wang, L. *et al.* 2004. Migration case study: Transport of radionuclides in a reducing clay sediment (TRANCOM-II). Nuclear Science and Technology Final Report **EUR 21022 EN**.
- Maes, N., Bruggeman, C., Govaerts, J., Martens, E., Salah, S. and Van Gompel, M. 2011. A consistent phenomenological model for natural organic matter linked migration of Tc(IV), Cm(III), Np(IV), Pu(III/IV) and Pa(V) in the Boom Clay. *Physics and Chemistry of the Earth, Parts A/B/C*, **36**, 1590–1599, <https://doi.org/10.1016/J.PCE.2011.10.003>
- Maes, N., Glaus, M. *et al.* 2021. State-of-the-art report on the understanding of radionuclide retention and transport in clay and crystalline Rocks. Final Version as of 30.04.2021 of Deliverable D5.1 of the HORIZON 2020 Project EURAD. EC grant agreement no. 847593.
- Martens, E., Maes, N., Weetjens, E., Van Gompel, M. and Van Ravestyn, L. 2010. Modelling of a large-scale in-situ migration experiment with ¹⁴C-labelled natural organic matter in Boom Clay. *Radiochimica Acta*, **98**, 695–701, <https://doi.org/10.1524/RACT.2010.1770>
- MATLAB 2020. Version 9.8. (R2020a), <https://www.mathworks.com>
- Mazurek, M., Alt-Epping, P. *et al.* 2011. Natural tracer profiles across argillaceous formations. *Applied Geochemistry*, **26**, 1035–1064, <https://doi.org/10.1016/J.APGEOCHEM.2011.03.124>
- Moulin, V.M., Moulin, C.M. and Dran, J.C. 1995. Role of humic substances and colloids on the behaviour of radiotoxic elements in relation with nuclear waste disposal: confinement or enhancement of migration? *American Chemical Society*, https://inis.iaea.org/Search/search.aspx?orig_q=RN:27045845
- ONDRAF/NIRAS 2013. Research, Development and Demonstration (RD&D) Plan, State-of-the-Art Report as of December 2012, **NIROND-TR 2013-12 E**.
- Porubcan, A.A. and Xu, S. 2011. Colloid straining within saturated heterogeneous porous media. *Water Research*, **45**, 1796–1806, <https://doi.org/10.1016/J.WATRES.2010.11.037>
- Put, M.J., Dierckx, A., Aertsens, M. and De Cannière, P. 1998. Mobility of the dissolved organic matter through intact Boom Clay cores. *Radiochimica Acta*, **82**, 375–378, <https://doi.org/10.1524/ract.1998.82.special-issue.375>
- Salah, S., Bruggeman, C. and Maes, N. 2015. Uranium retention and migration behaviour in Boom Clay: Topical Report – Status 2014, **SCKCEN-ER-305**. SCK•CEN Reports, <https://researchportal.sckcen.be/en/publications/uranium-retention-and-migration-behaviour-in-boom-clay-topical-re>
- Sen, T.K. and Khilar, K.C. 2006. Review on subsurface colloids and colloid-associated contaminant transport in saturated porous media. *Advances in Colloid and Interface Science*, **119**, 71–96, <https://doi.org/10.1016/J.CIS.2005.09.001>
- Sirivithayapakorn, S. and Keller, A. 2003. Transport of colloids in saturated porous media: a pore-scale observation of the size exclusion effect and colloid acceleration. *Water Resources Research*, **39**, <https://doi.org/10.1029/2002WR001583>
- Van Geet, M., Bastiaens, W. and Ortiz, L. 2008. Self-sealing capacity of argillaceous rocks: review of laboratory results obtained from the SELFRAC project. *Physics and Chemistry of the Earth, Parts A/B/C*, **33**, S396–S406, <https://doi.org/10.1016/J.PCE.2008.10.063>
- Van Laer, L. 2018. Long-term laboratory and in-situ migration experiments in Boom Clay – status 2017, **SCKCEN-ER-0390**, <https://researchportal.sckcen.be/en/publications/long-term-laboratory-and-in-situ-migration-experiments-in-boom-cl>
- Van Laer, L., Durce, D., Salah, S. and Maes, N. 2016. Sorption studies on Boom Clay and clay minerals – status 2016, **SCKCEN-ER-0346**. SCK•CEN Reports, <https://researchportal.sckcen.be/en/publications/sorption-studies-on-boom-clay-and-clay-minerals-status-2016>
- Weetjens, E. 2003. Technical note on modelling of the ²⁴¹Am–¹⁴C-labelled organic matter in Boom Clay. Technical Note prepared within the EC TRANCOM-II project contract no. FIKW-CT-2000-00008, 03/EWe/N-22&N-23.
- Weetjens, E., Maes, N. and Van Ravestyn, L. 2014. Model validation based on in situ radionuclide migration tests in Boom Clay: status of a large-scale migration experiment, 24 years after injection. *Geological Society, London, Special Publications*, **400**, 613–623, <https://doi.org/10.1144/SP400.39>
- Witte, R.S. and Witte, J.S. 2017. *Statistics*. 7th edn. John Wiley & Sons.
- Yu, L., Rogiers, B., Gedeon, M., Marivoet, J., De Craen, M. and Mallants, D. 2013. A critical review of laboratory and in-situ hydraulic conductivity measurements for the Boom Clay in Belgium. *Applied Clay Science*, **75–76**, 1–12, <https://doi.org/10.1016/J.CLAY.2013.02.018>
- Zsolnay, Á. 2003. Dissolved organic matter: artefacts, definitions, and functions. *Geoderma*, **113**, 187–209, [https://doi.org/10.1016/S0016-7061\(02\)00361-0](https://doi.org/10.1016/S0016-7061(02)00361-0)